Journal of Geophysical Research: Planets

RESEARCH ARTICLE
10.1029/2018JE005626

Key Points:
- The spatial, seasonal, and solar cycle variation of 10 years of Mars' TEC is assessed
- Mars Express routinely measures the dynamic of the thermosphere-ionosphere coupling
- The TEC can be used as a tracer for atmospheric cycles on the upper atmosphere

Spatial, Seasonal, and Solar Cycle Variations of the Martian Total Electron Content (TEC): Is the TEC a Good Tracer for Atmospheric Cycles?

Beatriz Sánchez-Cano[1], Mark Lester[1], Olivier Witasse[2], Pierre-Louis Blelly[3], Mikel Indurain[3], Marco Cartacci[4], Francisco González-Galindo[5], Álvaro Vicente-Retortillo[6], Andrea Cicchetti[4], and Raffaella Noschese[4]

[1]Radio and Space Plasma Physics Group, Department of Physics and Astronomy, University of Leicester, Leicester, UK, [2]European Space Agency, ESTEC-Scientific Support Office, Noordwijk, Netherlands, [3]Institut de Recherche en Astrophysique et Planétologie, Toulouse, France, [4]Istituto Nazionale di Astrofisica, Istituto di Astrofisica e Planetologia Spaziali, Rome, Italy, [5]Instituto de Astrofísica de Andalucía, CSIC, Granada, Spain, [6]Department of Climate and Space Sciences and Engineering, University of Michigan, Ann Arbor, MI, USA

Correspondence to:
B. Sánchez-Cano,
bscmdr1@leicester.ac.uk

Citation:
Sánchez-Cano, B., Lester, M., Witasse, O., Blelly, P.-L., Indurain, M., Cartacci, M., et al. (2018). Spatial, seasonal, and solar cycle variations of the Martian total electron content (TEC): Is the TEC a good tracer for atmospheric cycles? *Journal of Geophysical Research: Planets*, *123*, 1746–1759. https://doi.org/10.1029/2018JE005626

Received 24 MAR 2018
Accepted 24 MAY 2018
Accepted article online 31 MAY 2018
Published online 18 JUL 2018

Abstract We analyze 10 years of Mars Express total electron content (TEC) data from the Mars Advanced Radar for Subsurface and Ionospheric Sounding (MARSIS) instrument. We describe the spatial, seasonal, and solar cycle behavior of the Martian TEC. Due to orbit evolution, data come mainly from the evening, dusk terminator and postdusk nightside. The annual TEC profile shows a peak at Ls = 25–75° which is not related to the solar irradiance variation but instead coincides with an increase in the thermospheric density, possibly linked with variations in the surface pressure produced by atmospheric cycles such as the CO_2 or water cycles. With the help of numerical modeling, we explore the contribution of the ion species to the TEC and the coupling between the thermosphere and ionosphere. These are the first observations which show that the TEC is a useful parameter, routinely measured by Mars Express, of the dynamics of the lower-upper atmospheric coupling and can be used as tracer for the behavior of the thermosphere.

Plain Language Summary Ten years of Mars Express total electron content (TEC) data from the Mars Advanced Radar for Subsurface and Ionospheric Sounding (MARSIS) instrument are analyzed. The TEC is a parameter that gives information of the amount of free electrons within the ionosphere (ionized layer at ~100–200 km). In this study, we describe how the TEC varies along the seasons, planet coverage, and also with the solar activity. We have found that variations in the thermosphere (neutral atmospheric layer between 100 and 200 km) have an effect on the ionosphere, especially notable during spring of the northern hemisphere. With the help of a numerical simulation of the ionosphere-thermosphere over a Martian year, we have found that Mars' atmospheric cycles can have an effect on the upper atmosphere.

1. Overview

The Martian total electron content (TEC) has been the topic of several studies in recent times because of its potential to monitor the Martian ionospheric behavior (e.g., Cartacci et al., 2013, 2018; Lillis et al., 2010; Mendillo et al., 2013, 2015; Mendillo, Narvaez, & Campbell, 2017; Mendillo, Narvaez, et al., 2017; Morel et al., 2004; Safaeinili et al., 2007; Sánchez-Cano et al., 2016; Sánchez-Cano, Morgan, et al., 2015). The TEC represents the number of free electrons that are contained along the path between a radio transmitter and receiver. TEC at Mars is typically retrieved as a by-product of the analysis of the signal distortion caused by the dispersion that the ionosphere produces (e.g., Cartacci et al., 2013; Mouginot et al., 2008; Safaeinili et al., 2007). The above studies outlined the ionospheric variability and also highlighted the difficulty of relying on a very precise absolute number for the TEC at low solar zenith angles (SZA) on the pure dayside due to its dense ionosphere using the current radars at Mars, which have operating frequencies close to the peak plasma frequency.

Despite the progress made in the last decade, we still do not fully understand the long-term evolution of the ionospheric behavior in relation to the thermospheric variability. The ionosphere and thermosphere are obviously coupled because the ionosphere is formed by solar photoionization of the upper atmospheric

neutral layer, and governed by a variety of complex nonlinear chemical, dynamical, electrodynamical, and radiative processes (Yigit et al., 2016). The structure of the atmosphere-ionosphere system is influenced by several external and internal forcing processes, for example, space weather, crustal magnetic fields, or gravity waves among many others. New evidence demonstrates that different regions of the Martian atmosphere are fundamentally interconnected and behave as a unique coherent system (e.g., Bougher et al., 2015, 2017; Jakosky, 2015; Montmessin et al., 2017). This means that the whole atmospheric structure reacts together to external and internal sources of variability on different time and space scales. This is a growing topic largely unexplored so far.

In this study, we go one step further in order to assess whether the TEC is a useful tracer for the Martian thermosphere and, eventually, whether TEC can be used as a diagnostic parameter of the coupling between the lower and upper atmosphere. Specifically, we look into spatial, seasonal, and solar cycle effects of ~6 Martian years (MY; ~10 Earth years) of TEC observations from the Mars Advanced Radar for Subsurface and Ionospheric Sounding (MARSIS) instrument (Orosei et al., 2015; Picardi et al., 2004) onboard the Mars Express (MEX) mission, which has been in orbit about Mars since December 2003 (Chicarro et al., 2004).

This paper is divided as follows. In section 2, the general seasonal behavior of several relevant data sets for this study is described. In sections 3 and 4, the seasonal ionosphere-thermosphere coupling after considering the effect of the solar cycle is assessed for middle and polar latitudes, respectively. In section 5, a numerical simulation of the ionosphere is performed in order to help with the data interpretation. The simulation outlines the coupling between the ionosphere and the thermosphere as seen by the TEC observations. Finally, in section 6, the effect of the long-term coupling between the lower and upper atmospheres on the TEC is investigated, as this connection is much stronger than on Earth because Mars does not have a permanent stratosphere (e.g., González-Galindo et al., 2008).

2. General Observations

The ionosphere is characterized by a dynamic balance in which the net density of free electrons is described by the continuity equation, which depends on the relative speed of ion production and loss processes, and plasma transport (Chapman & Bartels, 1940). In addition, the ion production and ion losses depend on the intensity of the incoming solar radiation and on the density and chemistry of the neutral atmosphere (e.g., Witasse et al., 2008). At Earth, the solar flux is considered the dominant factor of ionization since the mass of the neutral atmosphere column, on average, does not vary significantly over a year for a given location. At Mars, beyond the irradiance flux, the thermosphere has a particular semiannual variation which may also have an influence on the ionospheric behavior with seasons, as we show in this section.

Figure 1 shows different ionospheric-atmospheric observations from several MY that have been averaged together and plotted with respect to the solar longitude (*Ls*), which can be used as a proxy for the MY. Each parameter in Figure 1 has been averaged within *Ls* bins of 10°. We note that results shown in this figure are not an artifact of the Ls binning process, because after using different sizes of *Ls* binning, similar results were obtained.

Figure 1a shows the averaged MARSIS TEC observations from ~6 MY (MY mid-27 to mid-32, mid-2005 to mid-2015) for a SZA of 85° (±0.5°). MARSIS TEC data come from its subsurface operational mode (Safaeinili et al., 2007). In this mode, the TEC is routinely estimated from the frequency phase shift caused by the ionosphere to the radar signals traveling from the spacecraft to the ground and vice versa (e.g., Sánchez-Cano, Morgan, et al., 2015). TEC was obtained through the Cartacci et al. (2013) algorithm, after only considering data with a signal-to-noise ratio (SNR) larger than 20 dB and only considering data from the two larger MARSIS frequencies, that is, 4 and 5 MHz. This conservative approach guarantees good quality data. We note that the SZA chosen in Figure 1a corresponds to a region near the terminator of the day. This is because the MARSIS radar in the subsurface mode is usually not operated on the full dayside due to low radar performance (Sánchez-Cano, Morgan, et al., 2015), and therefore, accurate TEC observations in the dayside are limited to high SZA. Moreover, the majority of the MARSIS data from SZA = 85° comes from the dusk sector, local time (LT)~18 h, due to the MEX orbit evolution and observation planning priorities. In an early MARSIS work with TEC data from 2005 to 2006, Safaeinili et al. (2007) showed that the ionosphere of Mars has a significant LT asymmetry. Unfortunately, due to the MEX orbit trajectory and science operation planning constrains and priorities over the subsequent years, it is not possible to do a similar analysis because

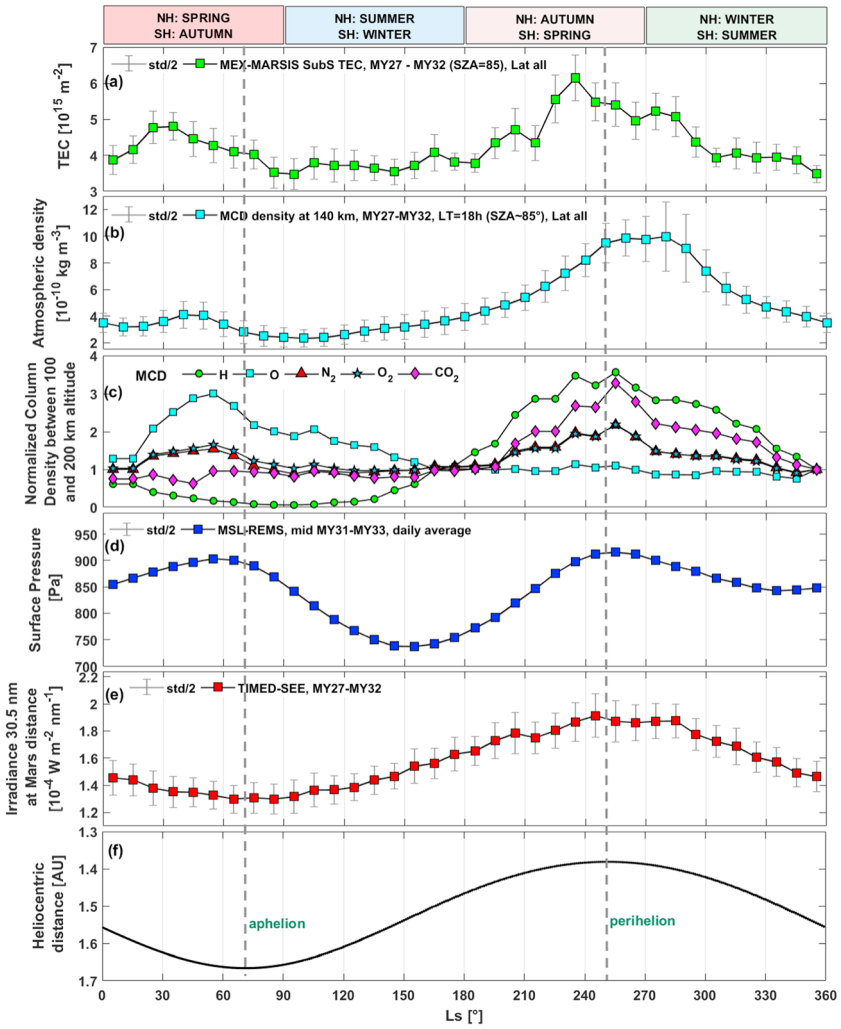

Figure 1. General annual observations. Each parameter in this figure has been averaged within *Ls* bins of 10° (squares). The half standard deviation of each *Ls* bins is shown with a grey vertical line. Mars' aphelion and perihelion are indicated with two vertical grey dashed lines. Northern hemisphere (NH) and southern hemisphere (SH) seasons are indicated at the top of the figure. (a) MEX MARSIS-TEC of MY 27–32 averaged over all latitudes and for SZA = 85°. (b) Averaged atmospheric density obtained from the MCD at 140 km for MY27–32 and all latitudes. Data in this panel vary according the solar flux of each day. (c) Temporal variability of the averaged MCD column density between 100 and 200 km and latitude for the major neutral species and normalized to their relevant value at *Ls* = 355° (see Figure 4). Data in this panel vary with a constant solar flux that is shaped only by the heliocentric distance. (d) MSL-REMS surface pressure average of mid MY 31–33. (e) TIMED-SEE solar irradiance for the 30.5-nm wavelength extrapolated to Mars's distance from MY 27 to 32. (f) Mars's heliocentric distance. MEX = Mars Express; MARSIS = Mars Advanced Radar for Subsurface and Ionospheric Sounding; TEC = total electron content; SZA = solar zenith angle; MCD = Mars Climate Database; MSL = Mars Science Laboratory; REMS = Rover Environmental Monitoring Station; MY = Martian years; TIMED = Thermosphere, Ionosphere, Mesosphere Energetics and Dynamics; SEE = solar EUV experiment.

the MARSIS dusk coverage is ~88% of the full data set, while the dawn coverage is only ~12%. Therefore, we consider that our results are not affected by the LT asymmetry, even if such asymmetry does exist (Safaeinili et al., 2007). Moreover, it is well known that the terminators are regions of localized high thermospheric variability (Zurek et al., 2017); the LT asymmetry is masked in this study as we statistically analyze 6 MY of TEC data together to assess the long-term evolution of the total ion and electron columns. Figure 1b shows the averaged atmospheric density at 140 km above the planet's surface (the approximate altitude of the maximum ionization region of the ionosphere) obtained from the Mars Climate Database (MCD). The MCD (version 5.3) is a meteorological database built from a Global Circulation Model (GCM) of the

Martian atmosphere, called Laboratoire de Meteorologie Dynamique (LMD) model, and widely validated with observational data (e.g., Forget et al., 1999; Millour et al., 2015). The MCD considers the CO_2, water, and dust cycles (Forget et al., 1998; Madeleine et al., 2012; Navarro et al., 2014) along with other meteorological conditions of each MY. In our case, Figure 1b shows the averaged results obtained from the MCD for the same period of the MARSIS TEC data (MY27–MY32) and after averaging the results from six equispaced different latitudes that cover the full planet. These data were obtained only at LT = 18 h, which corresponds to ~SZA = 85°, that is, the same condition as for the MARSIS TEC observations (Figure 1a) and with the actual solar flux conditions of those years. Figure 1c shows the global averaged thermospheric column density profile between 100- and 200-km altitude (i.e., the thermosphere) for each of the major species: hydrogen (H), atomic oxygen (O), molecular nitrogen (N_2), molecular oxygen (O_2), and carbon dioxide (CO_2). This figure does not show the relative abundances of the neutral species, but instead, it shows the temporal variability of each species, which has been normalized to its value at *Ls* = 355° in order to visualize all species on the same scale. Since the solar flux effect on the thermosphere can mask the annual variation of the neutral species, these profiles were obtained from the MCD after assuming a constant solar flux, as will be described in detail in the section 5. Figure 1d shows the daily averaged surface pressure measured by the Rover Environmental Monitoring Station (REMS) instrument (Gómez-Elvira et al., 2012) onboard the Mars Science Laboratory (MSL) mission (Grotzinger et al., 2012). The time span of this panel covers the ~3 MY that MSL has been working at the surface of Mars (MY mid-31 to -33, mid-2012 to beginning 2017). MSL is located almost near the Martian equator, and therefore, Figure 1d shows the averaged variation of the surface pressure (as a proxy for the atmospheric mass column variation) at almost equal distance from both poles. Figure 1e shows the solar irradiance measured by the Thermosphere, Ionosphere, Mesosphere Energetics and Dynamics (TIMED)-Solar Extreme Ultraviolet (EUV) Experiment (SEE) satellite (Woods & Eparvier, 2006) at a wavelength of 30.5 nm, which is the closest one measured by TIMED to the Helium 30.4-nm intense line of the spectrum that causes the major CO_2 ionization (main atmospheric component at Mars). The irradiance was measured at 1 AU for the same MARSIS TEC period (MY27–MY32) and subsequently extrapolated to Mars assuming that the irradiance was not significantly different in solar longitude when Earth and Mars were in superior solar conjunction. Finally, Figure 1f shows the Mars' heliocentric distance, illustrating aphelion at *Ls* = 71° and perihelion at *Ls* = 251°.

As expected, the TEC (Figure 1a) follows the irradiance profile well (Figure 1e) because the solar flux is the dominant agent of ionization. The sinusoidal shape of both the irradiance and the TEC is due to Mars' heliocentric distance (Figure 1f), as the solar flux diminishes with the square of the heliocentric distance. Therefore, both the TEC and the irradiance maxima are near Mars' perihelion and their minima near aphelion. However, the TEC profile shows a secondary maximum between *Ls* = 25° and 75° (Figure 1a), which is not related to the annual irradiance variation (Figure 1e). This feature was previously visible in Figure 3 of Hall et al. (2016), although its origin was not interpreted. This secondary peak occurs near the lowest solar irradiance level at Mars (Figure 1e), during the northern spring season and before aphelion, and nearly coincides with an increasing trend in both the thermospheric density (Figures 1b and 1c) and the surface pressure (atmospheric mass, Figure 1d). As seen in Figure 1c, when the solar flux is fixed as a constant, O, O_2, and N_2 have their largest abundances in the annual profile at this time of the year, indicating that these three components may have a more prominent role during this period, as we later analyze in more detail. Therefore, it seems that the thermosphere variability may play a role in the formation of this secondary TEC peak.

The main TEC peak (*Ls* = 220–290°) is also formed while there is an increase in the thermospheric density and surface pressure (during spring in the southern hemisphere), which is related to a larger abundance of CO_2, H, O_2, and N_2 with respect to their annual trends (Figure 1c). In this case, however, the solar irradiance is a maximum for this period (Figure 1e) and is the key factor in the formation of this TEC peak. As seen in Figure 1a, the absolute maximum of the MY occurs at *Ls* = 220–240°, a few *Ls* degrees before the irradiance maximum at *Ls* = 251°. Although not conclusive, this could also be a result of a neutral atmospheric effect, as the thermospheric conditions are similar to those regarding the first TEC peak, that is, spring in the southern hemisphere, increasing thermospheric density and increasing surface pressure, although with a much larger magnitude of the thermospheric density (Figure 1b) due to the expansion of the atmosphere produced by the proximity to the Sun (Figure 1f). However, it is difficult to evaluate whether there is an effect of the neutral atmosphere because the irradiance flux is clearly the dominant ionization factor and masks any other secondary ionospheric variability sources.

This overview figure demonstrates in a simple way the coherent long-term behavior of the thermosphere-ionosphere coupling, in which atmospheric changes may produce significant effects in the ionosphere formation. In the following section, we assess the long-term behavior of this coupling.

3. Ionosphere-Thermosphere Coupling: Middle-Low Latitudes

In order to assess the seasonal variability of the thermosphere-ionosphere coupling with latitude, SZA, and solar cycle, we have split the MARSIS data set by these parameters.

This section focuses only on TEC data from latitudes between −70° and 70°. Since Mars does not have a global intrinsic magnetic field such as Earth, there is no need to distinguish between low and middle latitudes because the ionospheric physics for all these latitudes is the same and can be analyzed together. We do not split the data set into smaller latitude bands because of data coverage constraints. Despite the long mission time of MEX, and hence the large amount of TEC data which have been acquired, there is a reduced latitude coverage in relation to the SZA coverage in a MY. This is a direct consequence of the MEX orbit evolution. Additionally, the MARSIS radar in subsurface mode only works during the ~30 min of the orbit's periapsis and when the SZA is high enough to avoid any radar signal losses due to a strong dayside ionosphere (Cartacci et al., 2018). Moreover, MARSIS switches between two operational modes, and so, it does not work in subsurface mode on all the orbits. For the same coverage reason, we show every single TEC observation as a dot in Figure 2 and not binned as in the previous figure.

In Figure 2, we present the TEC behavior of the Martian ionosphere in a year. The TEC data set has been split into intervals of 5° of SZA (rows), starting from SZA = [75°,80°] and ending with SZA = [110°,115°]. In addition, the TEC data set has been split into two different levels of solar activity based on the solar cycle classification made by Sánchez-Cano, Lester, et al. (2015) and Sánchez-Cano et al. (2016). The left column contains data from the low and medium solar activity phases of the solar cycle (MY mid-27 to mid-30, mid-2005 to early 2011), and the right column contains data from the high solar activity phase (MY mid-30 to -32, beginning 2011 to mid-2015). In order to achieve the best data coverage in each panel, the low and middle solar cycle phases in Sánchez-Cano, Lester, et al. (2015) and Sánchez-Cano et al. (2016) are considered as *low* in this work. This approximation is realistic as the solar irradiance levels were close enough during these three periods and remarkably different from the high solar activity phase (see Sánchez-Cano et al., 2016; Figure 1).

Data in each panel of Figure 2 have been fitted with a fifth degree polynomial curve (black dashed line) to visualize their averaged annual trend. The fifth-order polynomial has been chosen because it is the one that best reproduces the double TEC asymmetric peak shape, but its purpose is merely visual. Due to several data gaps between *Ls* 0° and 40°, the peak before aphelion (*Ls*~71°) is not visible with the fit in some panels, although the TEC rise in that sector can be discerned within the data. The thermosphere-ionosphere coupling effect (double TEC peak shape) is more remarkable during the high solar activity phase. During this phase, the ionosphere is denser due to larger EUV fluxes. This is manifested with a stronger Martian plasma obstacle to compete with the solar wind (e.g., Hall et al., 2016; Sánchez-Cano et al., 2016), and as it is shown in Figure 2, with a more intense coupling between the thermosphere and the ionosphere. Regarding its SZA dependence, the TEC observations show that the coupling in the dayside is stronger and becomes weaker as the nightside approaches (i.e., larger SZA). This coupling is maintained longer into the nightside, up to SZA~105° during the high solar activity phase, while it is only visible up to SZA~90° (day-night terminator) at the low solar activity phase. For larger SZA intervals there is no evidence for this atmospheric coupling in the ionosphere as seen with the TEC, since the TEC is on average almost constant for all *Ls*. This is expected as the ionosphere is very faint during the nightside (Withers et al., 2012) because the main photoionization source, the solar radiation, is not present. Regarding the time occurrence of both maxima, both are regularly observed at *Ls*~30–50° and 210–230° in all panels in which the coupling is observed. We note that the presence of crustal fields in the southern hemisphere, statistically, does not seem to have any distinguishable effect on these trends. Cartacci et al. (2013) showed that the TEC on the nightside shows a typical increase of 5% over the regions of quasi vertical magnetic fields, and a small decrease of 2% over the regions of quasi horizontal magnetic fields. Although significant, these variations are too small to affect our statistics where data from global coverage and for more than 10 years are averaged. We conclude that the annual occurrence of both TEC maxima is not dependent on solar conditions such as the SZA or the solar activity.

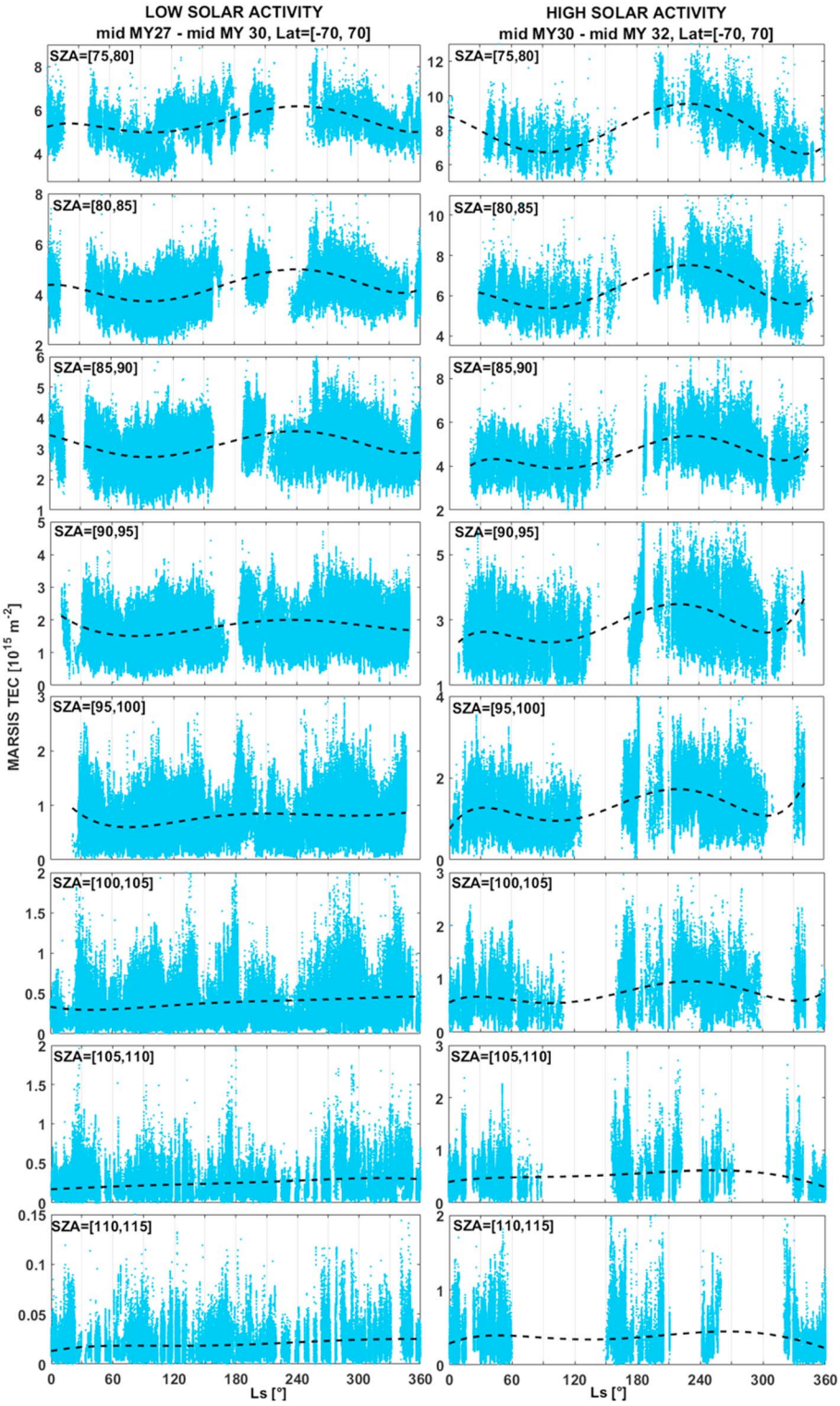

Figure 2. (left column) TEC of low solar activity period for increasing SZA. (right column) Same as left column for the high solar activity period. The dashed lines correspond to the best fit to the data. TEC = total electron content; SZA = solar zenith angle; MY = Martian years; MARSIS = Mars Advanced Radar for Subsurface and Ionospheric Sounding.

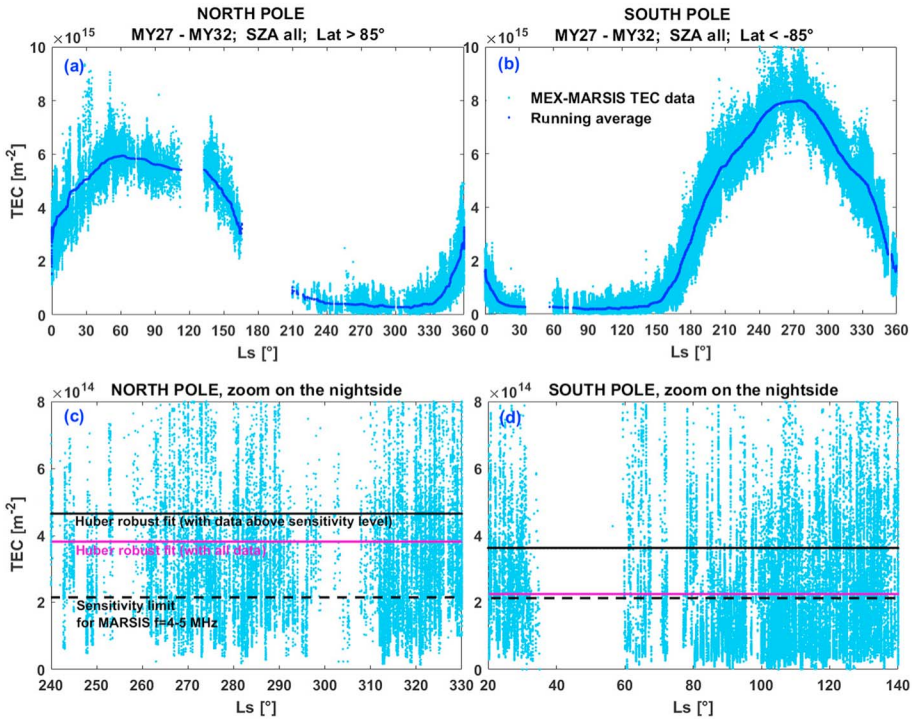

Figure 3. Annual TEC of the polar ionosphere. (a) North pole. (b) South pole. (c) Zoom on the north pole nightside. (d) Zoom on the south pole nightside. TEC = total electron content; MY = Martian years; MARSIS = Mars Advanced Radar for Subsurface and Ionospheric Sounding.

4. Ionosphere-Thermosphere Coupling: Polar Latitudes

Figure 3 shows the TEC behavior of the polar regions (latitudes larger than ±85°). These regions are two of the most sampled areas of the planet by the MARSIS radar, as the polar cap mapping was one of the mission priorities (Orosei et al., 2015). Consequently, the TEC data coverage of these regions is excellent. As on Earth, SZA and LT parameters do not have a daily key role at these latitudes. However, the main difference with Earth is that the Martian TEC only responds to solar irradiance changes and neutral atmospheric variations at these latitudes because Mars does not have a global internal magnetic field. Another important factor to consider is the heliocentric distance (Figure 1f), which results in different levels of solar irradiance when each pole is illuminated. The TEC maximum of the south pole is 1.3 times larger in magnitude than the north pole TEC maximum (Figures 3a and 3b) during the half-year polar dayside, which is coherent with the ratio of heliocentric distances of the perihelion and aphelion. We note that in this figure we have not distinguished between solar activity phases because we did not observe any significant TEC difference with the solar activity. The TEC maximum at the south pole is centered between the perihelion and the summer solstice (Ls = 251–270°), while in the north pole, it is centered at Ls = 50–80° around aphelion (Ls = 71°) and just before the summer solstice (similar Ls to the second TEC peak in Figure 1a).

During the approximately half-year nightside of each polar cap, the ionosphere is still present although very weak, maintained by processes such as dayside transport or electron precipitation (e.g., Fox et al., 1993). Figures 3c and 3d show the polar night ionosphere of each hemisphere, respectively. The dashed line indicates the sensitivity level of MARSIS, as calculated by Mouginot et al. (2008). To better visualize the averaged TEC values, we have performed two Huber robust fits (Huber, 1964), one to all the data that has previously passed the frequency and SNR selection criteria and another one only to the nightside data above the sensitivity level. If we consider first all the data, the nightside ionosphere of the north pole is ~1.7 times denser on average than both the south pole nightside ionosphere and the sensitivity level, indicating a weak but present ionosphere during all the half-year nightside. However, the nightside ionosphere of the south pole is faint, close to the sensitivity level. Considering only data above the sensitivity level, the ratio between the north and south pole nightside ionosphere is equal to 1.3. The MCD estimates that the column density during the north polar winter is 1.9 times larger than during the south polar winter, as calculated for the Ls and

latitude conditions of each polar night in Figure 3, for a LT of 18 h and longitude of 180°. Therefore, the measured ratio of the polar night electron densities is also coherent with the changes in the polar night thermospheric densities, as the electron density is proportional to the square root of the neutral density (Chapman, 1931). Additionally, another important process to consider is the day-night plasma transport and polar neutral winds that can have an effect on the level of ionization of each polar night. Since the winter in the north pole occurs while Mars is transiting its perihelion, plasma transport from the dayside regions of the ionosphere to the polar nightside could be larger than during winter in the south pole, which occurs at aphelion and when the dayside ionosphere is less robust because less solar irradiance reaches Mars.

5. Ionosphere-Thermosphere Simulation

To evaluate if variations of the neutral atmosphere are responsible for the seasonal TEC variations observed in the MARSIS data set, we have performed a numerical simulation of the ionosphere during a MY. We have used the Mars version of the numerical/physical model IRAP plasmasphere-ionosphere model (IPIM; Marchaudon & Blelly, 2015), which is an updated version of the TRANSCAR and TRANSMARS family of models (e.g., Blelly et al., 1996, 2005; Morel et al., 2004; Ramírez-Nicolás et al., 2016; Sánchez-Cano, Lester, et al., 2015; Witasse et al., 2002). The model is a physical description of the thermosphere and ionosphere of Mars using kinetic and fluid formalisms. The IPIM model can be run from the Transplanet's Space Weather Prediction Center (http://transplanet.cdpp.eu), which is a source for planetary space weather forecasts (André et al., 2017). Moreover, the Mars version of IPIM is coupled with the previously described MCD-LMD atmospheric model (version 5.3), which is used as input for the neutral atmosphere and it is currently one of the most up to date and used models of the atmosphere of Mars. The simulation was performed for 1 MY with SZA = 85° and LT 18 h in all latitudes (similar conditions to Figure 1a). The main difference is that the solar flux was kept constant, varying only with the heliocentric distance, for the entire simulation to avoid ionospheric variations due to changes in the solar activity that would mask the effect of the neutral atmosphere on the TEC results. The solar flux was fixed for the 8 February 2013 ($F_{10.7}$ = 104, medium solar activity conditions).

Outputs from the simulation are plotted in Figure 4 in the form of contour plots of latitude versus *Ls*. To produce these plots, outputs were gridded using a Triangulation-based linear interpolation, and only considered latitudes from which simulation outputs could be retrieved. The column density between 100 and 200 km of the major neutral species in Mars' thermosphere is plotted on the right column, which should be similar to the MCD outputs. At spring and summer in the northern hemisphere (*Ls* = 0–180°), the simulation shows that there is an increase in the thermospheric O_2, O, and N_2 column densities with respect to their respective values along the year, which mainly cover the period *Ls*~20–150°. There is also an increase in CO_2 in the northern hemisphere thermosphere but less significant than for the other molecules. On the other hand, there is a significant reduction of this molecule in the southern polar cap region, which may be related to the CO_2 condensation in the lower atmosphere due to the winter season in the southern hemisphere. At spring and summer in the southern hemisphere (*Ls* = 180–270°) something similar occurs, although the chemistry involved is slightly different. The thermospheric column density of CO_2, O_2, N_2, and H shows an increase between *Ls*~210° and 320° mainly in the southern polar cap which spreads to northern midlatitudes. These increases could be related to a warmer and thicker thermosphere (seasonal atmospheric expansion) due to a closer distance to the Sun.

The TEC and the contribution of different ions to the TEC are plotted on the left column. Due to electron neutrality

$$\mathrm{TEC}_{\mathrm{electrons}} = \sum_{i=1}^{n} \mathrm{TEC}_{\mathrm{ion}_i} \quad (1)$$

where *n* is the total number of ion species and *i* is the count of each one. The simulation shows that at northern spring (*Ls* = 0–90°), there is a significant increase in the TEC contribution from the ions O^+, O_2^+, and NO^+ in both hemispheres, NO^+ being mainly significant in the southern middle-latitude hemisphere. On the contrary, there is a significant decrease in the TEC contribution from the ion CO_2^+, especially in the southern polar cap which coincides with the CO_2 column density reduction. Near aphelion and the start of the northern summer (*Ls*~70–120°), there is a large reduction in the N_2^+, NO^+, and O_2^+ TEC contributions, which match with the TEC and irradiance minima for this period. At spring in the southern hemisphere (*Ls* = 180–270°), there is a global CO_2^+ increase, which coincides with O_2^+, N_2^+, and H^+ ion increases at the northern polar cap.

Figure 5 shows the contribution in percentage of each ion to the total TEC from the previous simulation. To get the contribution, each ion value has been divided by the corresponding TEC value for each *Ls* bin and

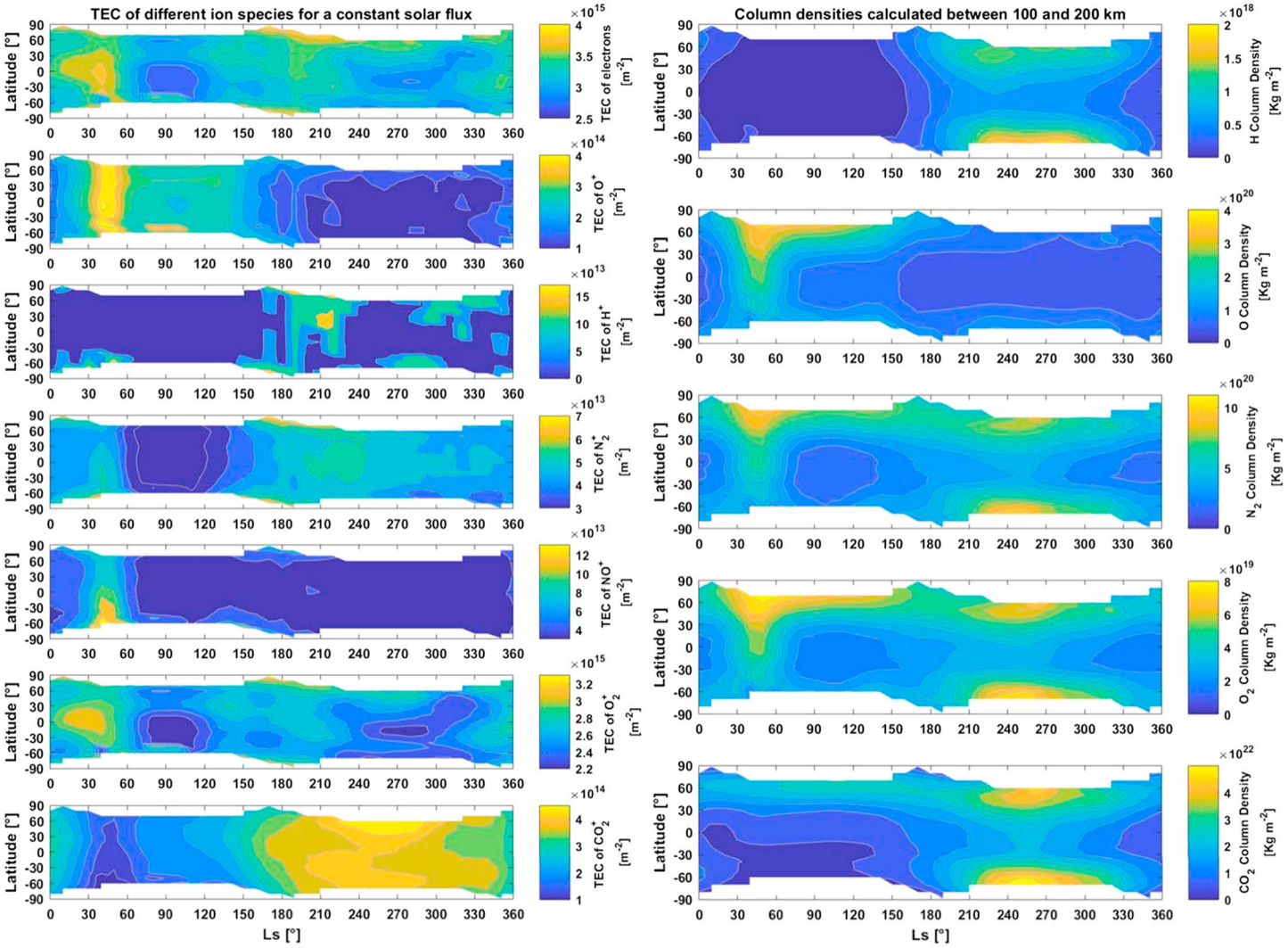

Figure 4. IPIM ionospheric simulations for SZA = 85°, local time 18 h, and a constant solar flux fixed for the day 8 February 2013. The IPIM model is coupled with the GCM-LMD model, whose outputs come from the Mars Climate Data set (MCD) 5.3 version. All the panels show the latitude evolution of the following parameters in a Martian year (via proxy *Ls*). (left column) TEC contribution of each of the main ion species. (right column) Column density between 100 and 200 km of each major neutral species. Note the different scale of the color bars. IPIM = IRAP plasmasphere-ionosphere model; SZA = solar zenith angle; GCM = Global Circulation Model; LMD = Laboratoire de Meteorologie Dynamique; TEC = total electron content.

multiplied by 100. Therefore, the annual TEC profile is a straight line at the 100% level. Three different latitude bands have been plotted, that is, the north pole region (latitudes>60°), the equator region (−10° < latitude<10°), and the south pole region (latitudes<−60°). For the three cases, as expected, the largest contribution to the TEC comes from the O_2^+ ion, which oscillates between the 77% and 82% (tending to be larger at *Ls*~0–180° and lower at *Ls*~180–360°). The second largest contribution comes from the O^+ and CO_2^+ ions (3–13%), which have the opposite behavior during the MY, that is, when one is maximum the other one is minimum, and vice versa. This is consistent from the chemistry point of view, because O_2^+, which is the major ion in the Martian ionosphere, is mainly formed via the reactions:

$$CO_2^+ + O \rightarrow O_2^+ + CO \quad (2)$$

$$O^+ + CO_2 \rightarrow O_2^+ + CO \quad (3)$$

For *Ls*~20–140°, the simulation indicates that the O^+ contribution to the TEC is 3–7% larger than that of CO_2^+ for the three latitude bands, having a maximum/minimum, respectively, at *Ls*~45°. On the other hand, the

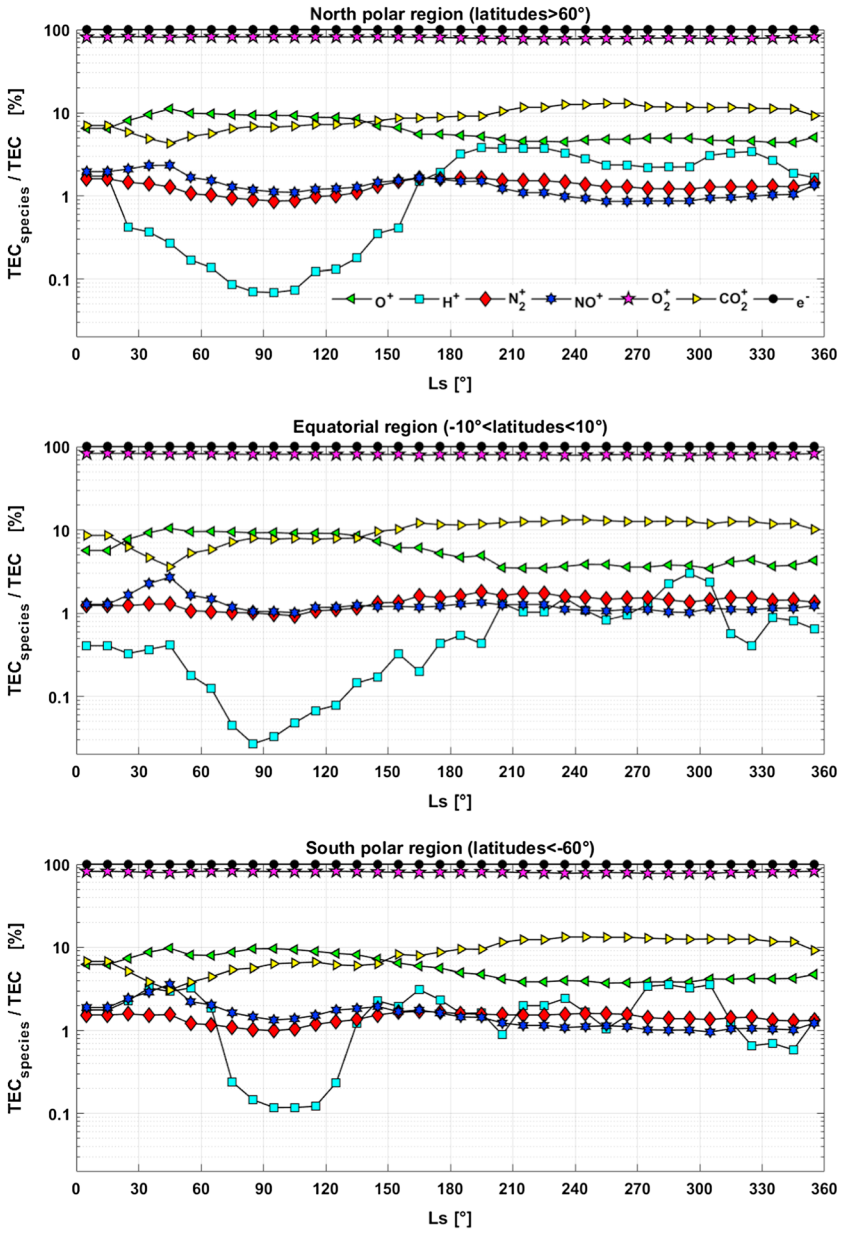

Figure 5. TEC contribution of each species for three different latitude bands, from the simulation of Figure 4. Each profile has been normalized by the corresponding TEC at each *Ls*. TEC = total electron content.

MCD model estimates that for the same *Ls* sector, the O column density has a peak 3 times larger than when compared to the last *Ls* bin of the year (Figure 1d), while the CO_2 column has almost no variation. Consequently, increased levels of atomic oxygen results in more O^+ ions to be produced. Then, the CO_2^+ loses by reaction with atomic oxygen is larger, and this is clearly observed in the CO_2^+ contribution to the TEC. The peak of O_2^+ which leads to the TEC peak is therefore explained by the increase of the two major production processes of this ion (equations (2) and (3)).

For *Ls*~140–360°, something different occurs. The main TEC peak (Figure 1a) is obviously formed by the maximum of solar flux (Figure 1e) and by the maximum neutral atmosphere column density (Figures 1 and 4). Considering only the atmospheric effect as in the simulation, the CO_2^+ contribution to the TEC is ~10% larger than the O^+ one, being almost constant from *Ls*~215–345°. For this *Ls* sector, the MCD model estimates that the O column density has almost no variation, while the CO_2 column density has a peak 3 times larger than when compared to the last *Ls* bin of the year (Figure 1d). Therefore, for this period of the year, increased levels

of CO_2 result in more CO_2^+ ions being produced, and as a result, O^+ is reduced. Following equations (2) and (3), the peak of O_2^+ (and so, the TEC) is formed.

Regarding other minor, but not negligible species, the simulation indicates that NO^+ and N_2^+ contribute to the total TEC, on average, less than 2%. NO^+ dominates over N_2^+ for $Ls < 150°$, having a peak in the three latitude bands at $Ls = 45°$. This peak is a 3.6% contribution to the TEC at the south polar regions, a 2.6% at the equator, and a 2.3% at the north polar regions. For $Ls > 150°$, N_2^+ dominates over NO^+ and its contribution to the TEC is almost a constant below a 2% level. Finally, the minor ion for $Ls < 150°$ is H^+, the contribution to the TEC of which can be considered, on average, negligible. However, for $Ls > 150°$, there is a significant increase of this ion, reaching the order of NO^+ and N_2^+ at the south pole and equator regions and ~2% larger at the north polar regions.

6. Discussion: Can TEC Be Considered as a Diagnostic Tool for the Coupling Between the Lower and Upper Atmosphere?

In this work, we have shown for the first time that the TEC routinely measured by MEX is an excellent indicator of the long-term variability of the thermosphere with latitude, SZA, seasons, and solar cycle phases. Moreover, it seems that it can also be a good indicator of the dynamics of the coupling between the lower and upper atmosphere. Numerous previous studies have shown different aspects of this coupling, such as planetary and tidal waves that move from the low atmosphere to the thermosphere (e.g., Bougher et al., 2001, 2004; Forbes et al., 2002), gravity waves (e.g., England et al., 2017), northern polar warming of the lower thermosphere near the perihelion/winter solstice (Bougher et al., 2006), the effect of the seasonal thermal expansion/contraction of the Mars lower atmosphere (e.g., Bougher et al., 2004), or the expansion of the entire atmosphere during dust storms (e.g., Keating et al., 1998). There are other processes that occur in the lower-middle atmosphere, such as atmospheric cycles of different species, which may propagate upward to the upper atmosphere, although this is a point in which we are still lacking a clear qualitative description.

An example is the CO_2 cycle, in which the mass of the atmosphere can vary up to 30% during seasons (e.g., James et al., 1992). This is a consequence of the CO_2 condensation that every winter occurs at high latitudes and the subsequent sublimation during the spring and summer seasons. This cycle induces a large semiannual variation in the daily averaged surface pressure all over the planet (Figure 1d; e.g., Forget et al., 2007; Martínez et al., 2017). Another case related to the CO_2 cycle is the water cycle in which water vapor is released into the atmosphere from the polar caps during spring and mainly summer when the CO_2 ice layer has disappeared and a water ice layer is exposed to the atmosphere. Then, this water vapor is transported equatorward by the atmosphere (Navarro et al., 2014; Trokhimovskiy et al., 2015), being a factor of 2 smaller during the southern hemisphere spring than during the northern hemisphere spring. During winter, both seasonal CO_2 polar caps act as a sink for any atmospheric water vapor (Harbele, 2003). Moreover, other species like O, O_2, or O_3 have been shown to have also a cyclic behavior during the year that somehow depend on these polar cap processes. The MEX-SPICAM instrument has shown the long-term evolution of these species below 50 km, which have a maximum of production during the northern spring season (see the review of Montmessin et al., 2017, and references therein). Specifically, O_3 shows a strong anticorrelation with water vapor, which makes the O_3 column density to be larger at high latitudes during early spring of each hemisphere and totally disappear during the summer seasons (e.g., Perrier et al., 2006).

We have shown in Figure 4 that for fixed solar conditions, there is a significant thermospheric increase of O, O_2, and N_2 molecules in the most northern latitudes during spring coinciding with the CO_2 sublimation period of the northern polar cap ($Ls = 0–70°$). The increase of these neutral species results in more N_2^+, O_2^+, O^+, and NO^+ ions in the ionosphere at all latitudes during this time of the MY, and therefore, in a significant TEC increase. This thermospheric variability, which is repeated every MY independently of the solar activity levels, is likely linked to atmospheric variability produced by cycles at lower atmospheric levels. Our results seem to be supported by the MEX-SPICAM observations of the lower atmosphere. Thermospheric O_2 column densities have similar increases both in latitude and Ls with respect to O_2 column density observations of the low-middle atmosphere (Figure 1 of Montmessin et al., 2017), being maximum in the early northern and southern springs in both hemispheres. As a consequence, the double peak in the TEC as a function of a MY could be the result of a larger increase in the column density of oxygen species, caused by the semiannual atmospheric cycles produced by the sublimation of the polar caps.

There are other seasonal factors that have been proved to have an effect on the thermosphere-ionosphere system. For example, there are typically large amounts of dust suspended in the lower atmosphere during the dust season (near the perihelion) that have a heating effect on the lower atmosphere (e.g., Bougher et al., 2001; Wang & Nielsen, 2003; Withers, 2009). This produces a thermal expansion of the lower atmosphere that is also observed in the upper atmosphere and as a consequence produces an increase in the altitude of the ionospheric peak (e.g., Hantsch & Bauer, 1990). Furthermore, Withers et al. (2015) recently reanalyzed the Mariner 9 radio-occultation profiles that were recorded during a severe global dust storm (Kliore et al., 1972) and found a similar result; the ionosphere was systematically lifted upward by 20–30 km, although the peak density of the ionosphere was not affected. These observations suggest that while the ionosphere/thermosphere system was only moved upward, the total electron/ion column density, the TEC, was not affected. In our case, since the TEC peak observed in Figure 1a occurred before aphelion (not in the dust storm season) and is always observed at different latitudes, dayside and solar cycle phases, we do not expect it to be a consequence of any of the above mentioned factors which lead to a lift of the atmosphere. Instead, as data and modeling suggest, the low-upper atmospheric coupling due to atmospheric cycles seems more plausible.

7. Conclusions

In this paper, we have shown for the first time that the TEC of the ionosphere is an interesting indicator of the dynamic of the thermosphere-ionosphere coupling and can be used as a tracer for the variability of the thermosphere. Using 10 years of MEX TEC observations, we have assessed the seasonal, latitudinal, and solar cycle variability of this coupling. The annual TEC profile closely follows the irradiance profile with a maximum near perihelion and a minimum near aphelion because the solar flux is the dominant factor for ionization as expected. However, the TEC annual profile shows an unexpected secondary maximum at Ls = 25–75°, which is not related to the annual irradiance variation. This is observed during the northern spring season and before aphelion and occurs together with an increase in both the thermospheric density and the surface pressure. These double peaks in the annual TEC profile occur always at the same Ls and are most likely a consequence of the seasonal variability of the thermosphere.

Moreover, we have performed a numerical simulation of the ionosphere-thermosphere of Mars with the IPIM model for a MY, under the constraint that the solar flux was kept constant for the full simulation, varying only with the heliocentric distance. The results show that the ion contribution to the TEC varies with season, being O^+ more important than CO_2^+ during the first part of the year (northern spring and summer) at all latitudes and CO_2^+ more important than O^+ during the second part of the year (northern autumn and winter). On average, both ion species have an equal contribution to the TEC at each half of the year. Seasonal change of these ions may be related to the lower atmosphere cycles, which produce a large semiannual mass atmospheric change with seasons. We show that this large amount of atmospheric mass variability could have a significant effect on the thermosphere and, therefore, on the ionosphere, especially near the aphelion of the Mars' orbit when the sublimation of the northern polar cap occurs and the solar irradiance is near the lowest value.

In conclusion, the TEC parameter, which is routinely measured by MEX since mid-2005, seems to be a promising tracer for the dynamic of the thermosphere-ionosphere coupling at least on the dayside region near terminator as supported by numerical simulations. Moreover, it seems to be a reliable indicator of the state of the lower-upper atmospheric coupling.

Acknowledgments

B. S. -C. and M. L. acknowledge support through STFC grant ST/N000749/1. ESA-ESTEC Faculty and Europlanet funding are also gratefully acknowledged. MEX MARSIS RDR and EDR data can be downloaded from the ESA-PSA archive, TIMED-SEE data at the University of Colorado's website (http://lasp.colorado.edu/lisird/index.html), REMS data at the NASA Planetary Data System (http://atmos.nmsu.edu/PDS/data/mslrem_1001/DATA/), the MCD model at the Mars Climate Database web interface (http://www-mars.lmd. jussieu.fr/mars/access. html), and the IPIM model at the IRAP CDPP web interface (http://trans-planet.irap.omp.eu/).

References

André, N., Grande, M., Achilleos, N., Barthélémy, M., Bouchemit, M., Benson, K., et al. (2017). Virtual planetary space weather services offered by the Europlanet H2020 research infrastructure. *Planetary and Space Science*, *150*, 50–59. https://doi.org/10.1016/j.pss.2017.04.020

Blelly, P. L., Lathuillère, C., Emery, B., Lilensten, J., Fontanari, J., & Alcaydé, D. (2005). An extended TRANSCAR model including ionospheric convection: Simulation of EISCAT observations using inputs from AMIE. *Annales de Geophysique*, *23*(2), 419–431. https://doi.org/10.5194/angeo-23-419-2005

Blelly, P.-L., Lilensten, J., Robineau, A., Fontanari, J., & Alcaýde, D. (1996). Calibration of a numerical ionospheric model with EISCAT observations. *Annales de Geophysique*, *14*(12), 1375–1390. https://doi.org/10.1007/s005850050399

Bougher, S. W., Bell, J. M., Murphy, J. R., Lopez-Valverde, M. A., & Withers, P. G. (2006). Polar warming in the Mars thermosphere: Seasonal variations owing to changing insolation and dust distributions. *Geophysical Research Letters*, *33*, L02203. https://doi.org/10.1029/2005GL024059

Bougher, S. W., Cravens, T. E., Grebowksy, J., & Luhmann, J. (2015). The aeronomy of Mars: Characterization by MAVEN of the upper atmosphere reservoir that regulates volatile escape. *Space Science Reviews*, *195*(1-4), 423–456. https://doi.org/10.1007/s11214-014-0053-7

Bougher, S. W., Engel, S., Hinson, D., & Murphy, J. (2004). MGS radio science electron density profiles: Interannual variability and implications for the Martian neutral atmosphere. *Journal of Geophysical Research*, *109*, E03010. https://doi.org/10.1029/2003JE002154

Bougher, S. W., Engel, S., Hinson, D. P., & Forbes, J. M. (2001). Mars Global Surveyor radio science electron density profiles: Neutral atmosphere implications. *Geophysical Research Letters*, *28*(16), 3091. https://doi.org/10.1029/2001GL012884

Bougher, S. W., Roeten, K. J., Olsen, K., Mahaffy, P. R., Benna, M., Elrod, M., et al. (2017). The structure and variability of Mars dayside thermosphere from MAVEN NGIMS and IUVS measurements: Seasonal and solar activity trends in scale heights and temperatures. *Journal of Geophysical Research: Space Physics*, *122*, 1296–1313. https://doi.org/10.1002/2016JA023454

Cartacci, M., Amata, E., Cicchetti, A., Noschese, R., Giuppi, S., Langlais, B., et al. (2013). Mars ionosphere total electron content analysis from MARSIS subsurface data. *Icarus*, *223*(1), 423–437. https://doi.org/10.1016/j.icarus.2012.12.011

Cartacci, M., Sánchez-Cano, B., Orosei, R., Noschese, R., Cicchetti, A., Witasse, O., et al. (2018). Improved estimation of Mars ionosphere total electron content. *Icarus*, *299*, 396–410. https://doi.org/10.1016/j.icarus.2017

Chapman, S. (1931). Absorption and dissociative or ionizing effects of monochromatic radiation in an atmosphere on a rotating Earth. *Proceedings of the Physical Society of London*, *43*(1), 26–45. https://doi.org/10.1088/0959-5309/43/1/305

Chapman, S., & Bartels, J. (1940). *Geomagnetism* (p. 1049). Oxford: Oxford University Press.

Chicarro, A., Martin, P., & Trautner, R. (2004). The Mars Express mission: An overview. In A. Wilson & A. Chicarro (Eds.), *Mars Express: The scientific payload* (Vol. 1240, pp. 3–13). Noordwijk, Netherlands: ESA Special Publication.

England, S. L., Liu, G., Yiğit, E., Mahaffy, P. R., Elrod, M., Benna, M., et al. (2017). MAVEN NGIMS observations of atmospheric gravity waves in the Martian thermosphere. *Journal of Geophysical Research: Space Physics*, *122*, 2310–2335. https://doi.org/10.1002/2016JA023475

Forbes, J. M., Bridger, A. F. C., Hagan, M. E., Bougher, S. W., Hollingsworth, J. L., Keating, G. M., & Murphy, J. R. (2002). Nonmigrating tides in the thermosphere of Mars. *Journal of Geophysical Research*, *107*(E11), 5113. https://doi.org/10.1029/2001JE001582

Forget, F., Hourdin, F., Fournier, R., Hourdin, C., Talagrand, O., Collins, M., et al. (1999). Improved general circulation models of the Martian atmosphere from the surface to above 80 km. *Journal of Geophysical Research*, *104*, 24,155–24,175.

Forget, F., Hourdin, F., & Talagrand, O. (1998). CO_2 snow fall on Mars: Simulation with a general circulation model. *Icarus*, *131*(2), 302–316. https://doi.org/10.1006/icar.1997.5874

Forget, F., Spiga, A., Dolla, B., Vinatier, S., Melchiorri, R., Drossart, P., et al. (2007). Remote sensing of surface pressure on Mars with the Mars Express/OMEGA spectrometer: 1. Retrieval method. *Journal of Geophysical Research*, *112*, E08S15. https://doi.org/10.1029/2006JE002871

Fox, J. L., Brannon, J. F., & Porter, H. S. (1993). Upper limits to the nightside ionosphere of Mars. *Geophysical Research Letters*, *20*, 1391–1394.

Gómez-Elvira, J., Armiens, C., Castañer, L., Domínguez, M., Genzer, M., Gómez, F., et al. (2012). REMS: The environmental sensor suite for the Mars Science Laboratory rover. *Space Science Reviews*, *170*(1-4), 583–640. https://doi.org/10.1007/s11214-012-9921-1

González-Galindo, F., Forget, F., Angelats, M., Coll, I., & López-Valverde, M. A. (2008). The Martian upper atmosphere. *Lecture Notes and Essays in Astrophysics*, *3*, 151–162.

Grotzinger, J. P., Crisp, J., Vasavada, A. R., Anderson, R. C., Baker, C. J., Barry, R., et al. (2012). Mars Science Laboratory mission and science investigation. *Space Science Reviews*, *170*(1-4), 5–56. https://doi.org/10.1007/s11214-012-9892-2

Hall, B. E. S., Lester, M., Sánchez-Cano, B., Nichols, J. D., Andrews, D. J., Edberg, N. J. T., et al. (2016). Annual variations in the Martian bow shock location as observed by the Mars Express mission. *Journal of Geophysical Research: Space Physics*, *121*, 11,474–11,494. https://doi.org/10.1002/2016JA023316

Hantsch, M. H., & Bauer, S. J. (1990). Solar control of the Mars ionosphere. *Planetary and Space Science*, *38*(4), 539–542. https://doi.org/10.1016/0032-0633(90)90146-H

Harbele, R. M. (2003). Planetary atmospheres: Mars. In *The encyclopedia of atmospheric science* (pp. 1745–1755). Academic Press. Retrieved from https://www.elsevier.com/books/encyclopedia-of-atmospheric-sciences/holton/978-0-08-052357-6

Huber, P. J. (1964). Robust estimation of a location parameter. *Annals of Mathematical Statistics*, *35*(1), 73–101. https://doi.org/10.1214/aoms/1177703732

Jakosky, B. M. (2015). MAVEN explores the Martian upper atmosphere. *Science*, *350*(6261), 643. https://doi.org/10.1126/science. aad3443

James, P. B., Kieffer, H. H., & Paige, D. A. (1992). The seasonal cycle of carbon dioxide on Mars. In *Mars* (pp. 934–968). Tucson, AZ: The University of Arizona Press.

Keating, G. M., Bougher, S. W., Zurek, R. W., Tolson, R. H., Cancro, G. J., Noll, S. N., et al. (1998). The structure of the upper atmosphere of Mars: In-situ accelerometer measurements from Mars Global Surveyor. *Science*, *279*(5357), 1672–1676. https://doi.org/10.1126/science.279.5357.1672

Kliore, A. J., Cain, D. L., Fjeldbo, G., Seidel, B. L., & Rasool, S. I. (1972). Mariner 9 S-band Martian occultation experiment: Initial results on the topography and atmosphere of Mars. *Science*, *175*(4019), 313–317. https://doi.org/10.1126/science.175.4019.313

Lillis, R. J., Brain, D. A., England, S. L., Withers, P., Fillingim, M. O., & Safaeinili, A. (2010). Total electron content in the Mars ionosphere: Temporal studies and dependence on solar EUV flux. *Journal of Geophysical Research*, *115*, A11314. https://doi.org/10.1029/2010JA015698

Madeleine, J.-B., Forget, F., Millour, E., Navarro, T., & Spiga, A. (2012). The influence of radiatively active water ice clouds on the Martian climate. *Geophysical Research Letters*, *39*, L23202. https://doi.org/10.1029/2012GL053564

Marchaudon, A., & Blelly, P.-L. (2015). A new 16-moment interhemispheric model of the ionosphere: IPIM. *Journal of Geophysical Research: Space Physics*, *120*, 5728–5745. https://doi.org/10.1002/2015JA021193

Martínez, G. M., Newman, C. N., De Vicente-Retortillo, A., Fischer, E., Renno, N. O., Richardson, M. I., et al. (2017). The modern near-surface Martian climate: A review of in-situ meteorological data from Viking to Curiosity. *Space Science Reviews*, *212*(1–2), 295–338. https://doi.org/10.1007/s11214-017-0360-x

Mendillo, M., Marusiak, A. G., Withers, P., Morgan, D., & Gurnett, D. (2013). A new semiempirical model of the peak electron density of the Martian ionosphere. *Geophysical Research Letters*, *40*, 5361–5365. https://doi.org/10.1002/2013GL057631

Mendillo, M., Narvaez, C., & Campbell, B. (2017). The total electron content of the Martian ionosphere from MRO/SHARAD observations. *Journal of Geophysical Research: Planets*, *122*, 2182–2192. https://doi.org/10.1002/2017JE005391

Mendillo, M., Narvaez, C., Matta, M., Vogt, M., Mahaffy, P., Benna, M., & Jakosky, B. (2015). MAVEN and the Mars Initial Reference Ionosphere model. *Geophysical Research Letters*, *42*, 9080–9086. https://doi.org/10.1002/2015GL065732

Mendillo, M., Narvaez, C., Vogt, M. F., Mayyasi, M., Mahaffy, P., Benna, M., et al. (2017). MAVEN and the total electron content of the Martian ionosphere. *Journal of Geophysical Research: Space Physics*, *122*, 3526–3537. https://doi.org/10.1002/2016JA023474

Millour, E., Forget, F., Spiga, A., Navarro, T., Madeleine, J.-B., Montabone, L., et al. (2015). The Mars Climate Database (MCD version 5.2), in European Planetary Science Congress 2015, vol. 10, EPSC2015–438, Nantes, France, 27 Sept.–2 Oct.

Montmessin, F., Korablev, O., Lefèvre, F., Bertaux, J.-L., Fedorova, A., Trokhimovskiy, A., et al. (2017). SPICAM on Mars Express: A 10 year in-depth survey of the Martian atmosphere. *Icarus*, *297*, 195–216. https://doi.org/10.1016/j.icarus.2017.06.022

Morel, L., Witasse, O., Warnant, R., Cerisier, J.-C., Blelly, P.-L., & Lilensten, J. (2004). Diagnostic of the dayside ionosphere of Mars using the total electron content measurement by the NEIGE/Netlander experiment: An assessment study. *Planetary and Space Science*, *52*(7), 603–611. https://doi.org/10.1016/j.pss.2003.12.007

Mouginot, J., Kofman, W., Safaeinili, A., & Herique, A. (2008). Correction of the ionospheric distortion on the MARSIS surface sounding echoes. *Planetary and Space Science*, *56*(7), 917–926. https://doi.org/10.1016/j.pss.2008.01.010

Navarro, T., Madeleine, J.-B., Forget, F., Spiga, A., Millour, E., Montmessin, F., & Maattanen, A. (2014). Global climate modeling of the Martian water cycle with improved microphysics and radiatively active water ice clouds. *Journal of Geophysical Research: Planets*, *119*, 1479–1495. https://doi.org/10.1002/2013JE004550

Orosei, R., Jordan, R. L., Morgan, D. D., Cartacci, M., Cicchetti, A., Duru, F., et al. (2015). Mars Advanced Radar for Subsurface and Ionospheric Sounding (MARSIS) after nine years of operation: A summary. *Planetary and Space Science*, *112*, 98–114. https://doi.org/10.1016/j.pss.2014.07.010

Perrier, S., Bertaux, J. L., Lefevre, F., Lebonnois, S., Korablev, O., Fedorova, A., & Montmessin, F. (2006). Global distribution of total ozone on Mars from SPICAM/MEX UV measurements. *Journal of Geophysical Research*, *111*, E09S06. https://doi.org/10.1029/2006JE002681

Picardi, G., Biccari, D., Seu, R., Plaut, J., Johnson, W. T. K., Jordan, R. L., et al. (2004). MARSIS: Mars advanced radar for subsurface and ionosphere sounding. In A. Wilson & A. Chicarro (Eds.), *Mars Express: The scientific payload* (Vol. 1240, pp. 51–69). Noordwijk, Netherlands: ESA Special Publication.

Ramírez-Nicolás, B., Sánchez-Cano, O., Witasse, P.-L., Blelly, L., & Vázquez, M. L. (2016). The effect of the induced magnetic field on the electron density vertical profile of the Mars' ionosphere: A Mars Express MARSIS radar data analysis and interpretation, a case study. *Planetary and Space Science*, *126*, 49–62. https://doi.org/10.1016/j.pss.2016.03.017

Safaeinili, A., Kofman, W., Mouginot, J., Gim, Y., Herique, A., Ivanov, A. B., et al. (2007). Estimation of the total electron content of the Martian ionosphere using radar sounder surface echoes. *Geophysical Research Letters*, *34*, L23204. https://doi.org/10.1029/2007GL032154

Sánchez-Cano, B., Lester, M., Witasse, O., Milan, S. E., Hall, B. E. S., Blelly, P.-L., et al. (2015). Evidence of scale height variations in the Martian ionosphere over the solar cycle. *Journal of Geophysical Research: Space Physics*, *120*, 10,913–10,925. https://doi.org/10.1002/2015JA021949

Sánchez-Cano, B., Lester, M., Witasse, O., Milan, S. E., Hall, B. E. S., Cartacci, M., et al. (2016). Solar cycle variations in the ionosphere of Mars as seen by multiple Mars Express datasets. *Journal of Geophysical Research: Space Physics*, *121*, 2547–2568. https://doi.org/10.1002/2015JA022281

Sánchez-Cano, B., Morgan, D. D., Witasse, O., Radicella, S. M., Herraiz, M., Orosei, R., et al. (2015). Total electron content in the Martian atmosphere: A critical assessment of the Mars Express MARSIS data sets. *Journal of Geophysical Research: Space Physics*, *120*, 2166–2182. https://doi.org/10.1002/2014JA020630

Trokhimovskiy, A., Fedorova, A., Korablev, O., Montmessin, F., Bertaux, J.-L., Rodin, A., & Smith, M. D. (2015). Mars' water vapor mapping by the SPICAM IR spectrometer: Five Martian years of observations. *Icarus*, *251*, 50–64. https://doi.org/10.1016/j.icarus.2014.10.007

Wang, J.-S., & Nielsen, E. (2003). Behavior of the Martian dayside electron density peak during global dust storms. *Planetary and Space Science*, *51*(4–5), 329–338. https://doi.org/10.1016/S0032-0633(03)00015-1

Witasse, O., Cravens, T., Mendillo, M., Moses, J., Kliore, A., Nagy, F., & Breus, T. (2008). Solar system ionospheres. *Space Science Reviews*, *139*(1-4), 235–265. https://doi.org/10.1007/s11214-008-9395-3

Witasse, O., Dutuit, O., Lilensten, J., Thissen, R., Zabka, J., Alcaraz, C., et al. (2002). Prediction of a CO^{2+} layer in the atmosphere of Mars. *Geophysical Research Letters*, *29*(8), 1263. https://doi.org/10.1029/2002GL014781

Withers, P. (2009). A review of observed variability in the dayside ionosphere of Mars. *Advances in Space Research*, *44*(3), 277–307. https://doi.org/10.1016/j.asr.2009.04.027

Withers, P., Fillingim, M. O., Lillis, R. J., Häusler, B., Hinson, D. P., Tyler, G. L., et al. (2012). Observations of the nightside ionosphere of Mars by the Mars Express Radio Science Experiment (MaRS). *Journal of Geophysical Research*, *117*, A12307. https://doi.org/10.1029/2012JA018185

Withers, P., Weiner, S., & Ferreri, N. R. (2015). Recovery and validation of Mars ionospheric electron density profiles from Mariner 9. *Earth, Planets and Space*, *67*(1), 194. https://doi.org/10.1186/s40623-015-0364-2

Woods, T. N., & Eparvier, F. G. (2006). Solar ultraviolet variability during the TIMED mission. *Advances in Space Research*, *37*(2), 219–224. https://doi.org/10.1016/j.asr.2004.10.006

Yigit, E., Koucka, P., Georgieva, K., & Ward, W. (2016). A review of vertical coupling in the atmosphere-ionosphere system: Effects of waves, sudden stratospheric warmings, space weather, and of solar activity. *Journal of Atmospheric and Solar - Terrestrial Physics*, *141*, 1–12. https://doi.org/10.1016/j.jastp.2016.02.011

Zurek, R. W., Tolson, R. A., Bougher, S. W., Lugo, R. A., Baird, D. T., Bell, J. M., & Jakosky, B. M. (2017). Mars thermosphere as seen in MAVEN accelerometer data. *Journal of Geophysical Research: Space Physics*, *122*, 3798–3814. https://doi.org/10.1002/2016JA023641